JOURNAL OF GEOPHYSICAL RESEARCH: OCEANS, VOL. 118, 1–14, doi:10.1002/jgrc.20131, 2013

Seasonal variability and coastal upwelling near Cape Santa Marta (Brazil)

Paula C. Campos,[1] Osmar O. Möller Jr.,[1] Alberto R. Piola,[2,3,4] and Elbio D. Palma[5,6]

Received 30 August 2012; revised 8 January 2013; accepted 18 February 2013.

[1] The Santa Marta Grande Cape (CSM) area, a relatively steep and narrow continental shelf off southeast Brazil, is under the influence of the Brazil Current and intense seasonal variations of the wind field that affect the composition of water masses and their circulation. Hydrographic data, satellite-derived wind stress, and numerical simulations are used to characterize the seasonal and shorter period variability of the oceanographic conditions off CSM, in the area between 27°S and 30°S. The study is focused on the upwelling episodes and the dynamical mechanisms associated with these events. Field data and numerical results indicate significant seasonal changes in the oceanographic structure, the water mass composition, and the dynamical balance. During fall and winter, when southwesterly winds prevail and the frequency of meteorological frontal systems increases, the region is characterized by waters of continental origin, the Plata Plume Water (PPW). During spring and summer, deeper waters reach the surface layer due to the action of northeasterly winds. Coastal upwelling events are revealed by surface temperature minima observed south of CSM. Synoptic data show that these events occur in pulses associated with changes in the wind direction. Analysis of the numerical results shows that this particular location of the upwelling band results from the synergy between shelf-break upwelling and the regional shelf circulation induced by the northeasterly winds, both of which are modulated by changes in the coastline orientation and shelf width.

Citation: Campos, P. C., O. O. Möller Jr., A. R. Piola, and E. D. Palma (2013), Seasonal variability and coastal upwelling near Cape Santa Marta (Brazil), *J. Geophys. Res. Oceans*, *118*, doi:10.1002/jgrc.20131.

1. Introduction

[2] Upwelling events are generally observed around capes along the southeastern Brazilian shelf [*Campos et al*., 1995; *Rodrigues and Lorenzetti*, 2001], among them capes São Tomé (CST, 22°S), Frio (CF, 23°S), São Vicente (CSV, 24°S), and Santa Marta Grande (CSM, 29°S Figure 1).

[3] Several studies have discussed the CF upwelling system, where the surface temperature can drop from 23°C to 15°C and nitrate concentration can rise from 4 to 10 μmol l^{-1}. South Atlantic Central Water (SACW) upwells in response to NE winds [*Guimaraens and Coutinho*, 2000; *Rodrigues and Lorenzzetti*, 2001]. The temperature variability around CF has been associated with Ekman transport caused by NE and SW winds [*Miranda*, 1982]. Wind and wind stress curl variability are also important in the development of upwelling and downwelling cycles [*Carbonel* 2003; *Castelão and Barth* 2006]. Though upwelling around CF has been reported in winter [*Moser and Gianesella-Galvão*, 1997], the more frequent and intense events are observed in summer and spring. The later events can influence the position of the Brazilian sardine spawning areas [*Matsuura*, 1998] and the algal distribution [*Guimaraens and Coutinho*, 2000].

[4] In contrast, there is limited knowledge on the role of upwelling events on the coastal ecosystem around CSM (Figure 1). North of CSM, the coast follows a N-S orientation, while farther south, it is oriented NE-SW. At CSM, the continental shelf is relatively narrow (~100 km), and the 50 m isobath is only 5 km away from the coast, while farther north and south, the shelf width increases. Most of the studies in this area have focused on the analysis of specific cruise profiles. Based on the analysis of historical oceanographic data, *Castello and Möller* [1977] first suggested that NE winds could lead to upwelling events in the region of CSM. The analysis of monthly conductivity-temperature-depth (CTD) profiles carried out by *Matsuura* [1986] also concluded that the cross-shore water mass structure observed in January 1978 was due to an upwelling event. Based on samples collected four times a day during a 7 day period, *Odebrecht and Djurfelt* [1996] described the

[1]Laboratório de Oceanografia Costeira e Estuarina, Instituto de Oceanografia, Universidade Federal do Rio Grande, Rio Grande-RS, Brazil.
[2]Departamento Oceanografia, Servicio de Hidrografia Naval, Buenos Aires, Argentina.
[3]Departamento Ciencias de La Atmósfera y los Océanos, Universidad de Buenos Aires, Buenos Aires, Argentina.
[4]UMI-IFAECI, CNRS/CONICET, Buenos Aires, Argentina.
[5]Departamento de Física, Universidad Nacional del Sur, Bahía Blanca, Argentina.
[6]Instituto Argentino de Oceanografía, CONICET, Bahía Blanca, Argentina.

Corresponding author: P. C. Campos, Laboratório de Oceanografia Costeira e Estuarina, Instituto de Oceanografia, Universidade Federal do Rio Grande, Av. Italia Km. 8, 96201-900, Rio Grande-RS, Brazil. (oceano.paula@gmail.com)

2169-9275/13/10.1002/jgrc.20131

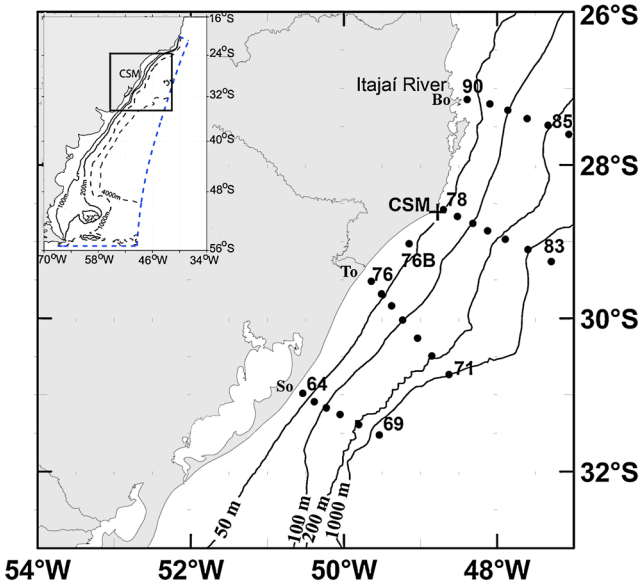

Figure 1. Southeastern shelf area depicting Cape Santa Marta Grande (CSM). The location of the Plata summer cruise hydrographic stations (dots) and the CSM time series (cross) are indicated. The numbers indicate the hydrographic stations. The black lines indicate isobaths from the GEBCO 1′ resolution bathymetry. So, To, and Bo are the cities of Solidão, Torres, and Bombinhas, which refer to the Plata cruise transects. The smaller panel shows the limits of the numerical model region of study. The black lines indicate the 100 and 200 m isobaths, and the black dashed lines indicate the 1000 and 4000 m isobaths.

evolution of stratification during upwelling and downwelling events. The observed changes were associated with the alternation of NE and SW winds due to the passage of a cold front. For both situations, they found that nutrient injection into the euphotic zone was driven by bottom turbulence, which presumably explained the observation of a subsurface chlorophyll *a* maximum. The high zooplankton biomass present in this area has been also associated with the influence of cold South Atlantic Central Water (SACW) [*Resgalla et al*., 2001].

[5] The presence of SACW in the bottom layer of the South Brazil Bight (SBB, ~28°S to 23°S) has been associated to shelf-break upwelling forced by the poleward flow of the Brazil Current (BC) in the outer shelf. *Campos et al*. [2000] and *Castelão et al*. [2004] ascribed the SBB shelf-break upwelling to the passage of meanders and eddies produced by instabilities of the BC. However, recent numerical simulations have suggested that shelf-break upwelling is a persistent feature of the regional circulation driven by the dynamical interaction between the BC and the SBB coastline orientation and shelf width [*Palma and Matano*, 2009]. The different models of upwelling are not mutually exclusive but, in fact, might reinforce each other. Once on the shelf, SACW might be brought to the surface under upwelling favorable winds.

[6] *Möller et al*. [2008] described an upwelling structure based on the analysis of CTD data collected along a cross-shore section occupied off CSM during summer (see Figure 1). Data were collected after a period preceded by several days of NE winds. Associated with the upwelling event, the presence of SACW at the surface is clearly depicted in the coastal region south of the cape. In agreement with these measurements, previous numerical simulations of the southern Brazilian Shelf also showed that upwelling might be intensified south of the cape [*Palma et al*., 2008]. *Möller et al*. [2008] also concluded that the upwelling of SACW requires the southward advection of low-salinity Plata Plume Water (*PPW*) that occupies a large portion of the shelf in winter. However, and although at a regional scale the most abrupt changes in shelf width and orientation occur at CSM, those previous studies did not specifically address the dynamic effects of these changes and its influence on the magnitude of the shelf-break upwelling, the shelf circulation, and the observed coastal upwelling events.

[7] The aim of this paper is to characterize the seasonal and higher frequency variability of the oceanographic conditions around CSM (between 27°S and 30°S—Figure 1) with emphasis on upwelling episodes and on the dynamical mechanisms associated with these events. To this end, we investigate the effects of wind forcing, discuss the role of changes in bottom topography and coastal orientation, and explain why the observed upwelling center is located south of the cape. To achieve these goals, we used three different data sets. In section 2, we describe the data and methods. In sections 3 and 4, we present the results and discussion. The conclusions are summarized in section 5.

2. Data and Methods

2.1. Data

[8] CTD profiles obtained during the Plata cruises (see Figure 1 for reference) [Campos *et al.*, 2008] are used to describe and compare the winter and summer situations and to validate the model results. These cruises sampled the continental shelf from Mar del Plata (Argentina) to Bombinhas (Brazil) in August 2003 (R/V *Puerto Deseado*) and February 2004 (R/V *Antares*). The area near CSM, between Solidão (31°S—So in Figure 1) and Bombinhas (27°S—Bo in Figure 1), was sampled between 29 August and 1 September 2003 and from 12 to 17 February 2004. Information about data sampling and processing procedures for these cruises is given by *Piola et al*. [2008a, 2008b] and *Möller et al*. [2008]. The thermohaline intervals for each water mass, used as reference in the analysis, were defined following *Piola et al*. [2000] and are presented in Table 1.

[9] The shorter period variability is analyzed based on a time series prepared from a repeated hydrographic station occupied from 23 to 30 October 1973 from the R/V *Alte. Saldanha* at the 50 m isobath, off CSM (28°37′12″S, 48°46′54″W). During this period, a total of 60 Nansen bottle

Table 1. Termohaline (TH) Intervals for Winter and Summer Used to Characterize the Water Masses (Defined According to *Piola et al*. [2000])

	Winter TH Interval	Summer TH Interval
PPW	$T > 10°C$, $S \leq 33.5$	$T > 20°C$, $S \leq 33.5$
TW	$T \geq 18.5°C$, $S \geq 36$	$T \geq 18.5°C$, $S \geq 36$
STSW	$T > 14°C$, $33.5 < S < 35.3$ $T > 18.5$, $35.3 \leq S < 36$	$T > 18.5°C$, $35.3 < S < 36$ $T > 21°C$, $33.5 < S \leq 35.3$
SACW	$T \leq 18.5°C$, $S \geq 35.3$	$T \leq 18.5°C$, $S \geq 35.3$

casts were taken at 3 h intervals. Each cast consisted of water samples and reversing thermometer readings collected at five standard depths.

[10] The wind can drive upwelling by two distinct mechanisms. First, alongshore wind stress can drive water offshore in the surface Ekman layer, forcing cold, nutrient-rich water, toward the surface. We refer to this process as Ekman transport [e.g., *Smith*, 1968]. Second, the wind stress curl generates surface divergence, forcing water upward, referred to as Ekman pumping [*Smith*, 1968]. These two contributions to the coastal upwelling were estimated following *Pickett and Paduan* [2003] based on QuikSCAT wind data spanning the period from 2003 to 2007 (available at ftp://podaac.jpl.nasa.gov/pub/ocean_wind/quikscat/L3/data). The wind stress time series were extracted from valid pixels along the coast located as close as possible to the shore. The Ekman transport contribution (in $m^3\ s^{-1}\ m^{-1}$ in the alongshore direction) was calculated as

$$M_x = \frac{\tau_y}{\rho_w f} \tag{1}$$

where τ_y is the alongshore component of the wind stress vector, ρ_w is the density of seawater (assumed constant at 1024 kg m^{-3}), and f is the Coriolis parameter. The alongshore component was defined in the N-S direction north of CSM and NE-SW (45° orientation) south of the cape. The contribution of the wind stress curl (the Ekman pumping velocity in m s^{-1}) was calculated as follows:

$$w = \frac{1}{\rho_w f} \nabla \times \tau \tag{2}$$

where $\nabla \times \tau$ is the curl of the wind stress. To estimate the transport associated with Ekman pumping, vertical velocities were integrated out to 100 km offshore (approximately the distance offshore where the negative wind stress curl extends).

2.2. Numerical Model

[11] The numerical model used is the Princeton Ocean Model [*Blumberg and Mellor*, 1987], adapted to the region which extends from 55°S to 23°S and from 70°W to 40°W. The horizontal model grid is designed using an orthogonal coordinate transformation with a total of 250 (along-shelf) × 150 (cross-shelf) grid points, which provides a horizontal resolution of about 5–20 km in the cross-shelf direction and 7.5–10 km in the along-shelf direction. The vertical resolution comprises 25 sigma levels, with a higher resolution within the surface and bottom boundary layers. The model topography over the shelf was obtained from nautical charts from the Argentine Hydrographic Service, supplemented with the 2′ resolution *Smith and Sandwell* [1997] topography for regions deeper than 250 m. The model has three open boundaries at the southern, western, and northern sides of the domain where we used a combination of radiation and advection boundary conditions recommended by *Palma and Matano* [1998, 2000]. Along the open boundaries, the model was forced with tidal amplitudes and phases predicted by the global 0.5° resolution TPXO.5 tidal model from Oregon State University [*Egbert et al*., 1994] and inflows from the Parallel Ocean Climate Model 4 eddy-permitting global ocean model [*Tokmakian and Challenor*, 1999]. The model was also forced at the ocean surface with wind stress values from the Scatterometer Climatology of Ocean Winds (SCOW) data base [*Risien and Chelton*, 2008], while surface heat and freshwater fluxes were handled through relaxation to climatological sea surface temperature (SST) and sea surface salinity. The model includes the freshwater discharges from the Rio de la Plata (Plata hereafter) (23,000 $m^3\ s^{-1}$) [*Piola et. al*., 2008a] and the *Patos Lagoon* (2,000 $m^3\ s^{-1}$) [Vaz *et al*., 2006]. The model was initialized with the Levitus annual mean temperature and salinity and spun-up for 3 years. After this period, climatological forcing was turned on, and the model was run for another 6 years. In this study, we analyzed the last of 3 years of simulation (E1). Another experiment (E2), initialized as E1 but without tidal and wind forcing, was used for the purposes of dynamical analysis. Other details about the model formulation can be found in *Palma et al*. [2008]. This model has been tested in previous studies of the shelf circulation [*Palma et al*.; 2008; *Palma and Matano*, 2009]. In the present study, we focus on the area extending from 25°S to 35°S and from 53°W to 45°W.

3. Results

3.1. Plata Cruises: A Comparison of Winter and Summer Oceanographic Situations

3.1.1. Surface Distribution

[12] Figure 2 displays the surface temperature and salinity distributions obtained during Plata cruises carried out in winter 2003 (Figures 2a and 2b) and summer 2004 (Figures 2c and 2d). In winter, the coastal region is dominated by low temperature (T<16°C, Figure 2a) and salinity ranging from 32 to 33.5 (Figure 2b), which indicate the presence of the PPW. The 33.5 isohaline, highlighted in Figure 2, indicates that the upper limit for PPW [*Möller et al*., 2008] is found at a distance of 120 km from the coast.

[13] In summer (Figures 2c and 2d), a low-temperature and high-salinity ($T < 18$°C, $S > 35.5$) region is observed near the coast at 29°S, suggesting upwelling. The offshore edge of this region is marked by a sharp temperature front with temperature rapidly increasing offshore (SST > 24°C). The upwelling core is located south of the cape. This area was sampled during a period of NE winds that had blown for 10 successive days from 5 to 15 February 2004 before rotating to the SW due to the passage of a frontal system [*Möller et al*., 2008].

3.1.2. Vertical Structure

[14] To gain further insight on the seasonal differences, in Figure 3, we present cross sections of temperature, salinity, and density (σ_θ) off CSM (stations 78–83 in Figure 1). The winter profiles reveal that temperature, salinity, and density (Figures 3a–3c, respectively) increase offshore. Near the coast, low temperature ($T < 18$°C) and salinity ($S < 33.5$) are associated with the PPW (see Table 1 for reference) that occupies a large portion of the continental shelf and extend to the bottom in the inner 20 km. Below 100 m depth, the 18°C isotherm and the 36 isohaline mark the limit between Tropical Water (TW) and SACW. The thermohaline gradient observed in the PPW-TW transition ($T > 18$°C and $S > 36$) is the Subtropical Shelf Water (STSW) that results from the lateral mixing between these two water masses [*Piola et al*., 2000, 2008a]. TW located between

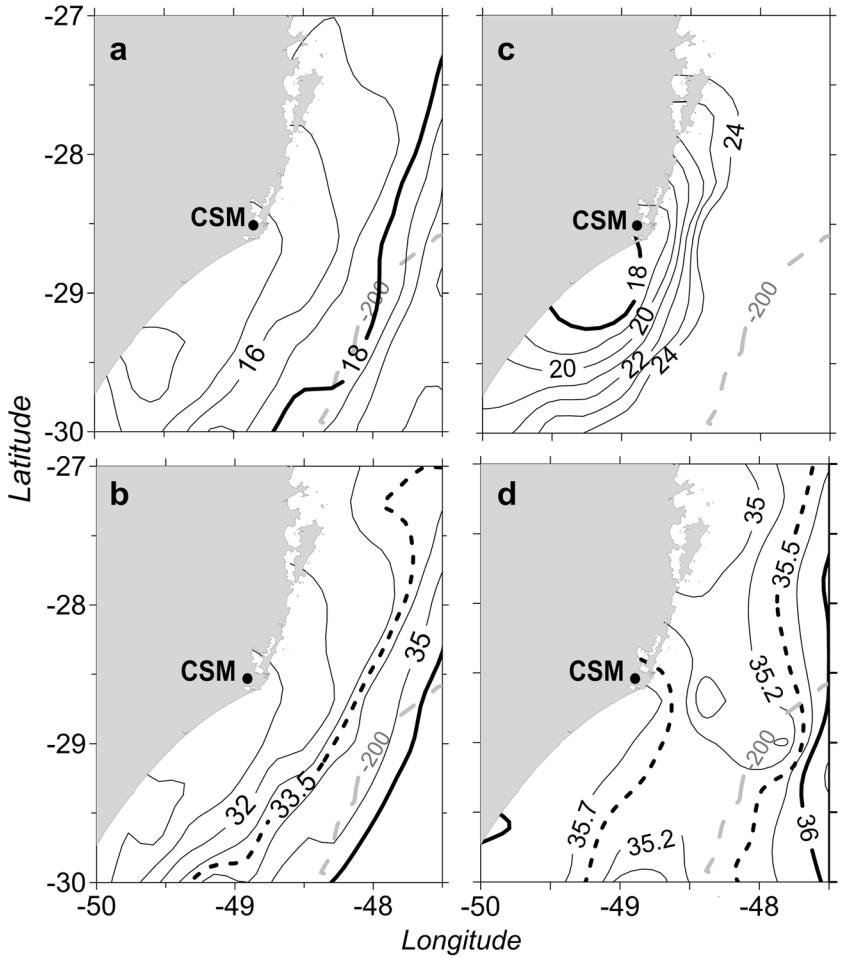

Figure 2. Surface temperature and salinity distribution for (a, b) winter of 2003 and (c, d) summer of 2004. In winter, the 18°C isotherm (heavy) and the 33.5 isohaline (dashed) indicate PPW. In summer, the 18°C isotherm and 35.5 isohaline (dashed) indicate SACW. The 36 isohaline (heavy line) indicates the lower TW limit. The gray dashed line indicates the 200 m isobath.

PPW and SACW and the vertical extent of PPW on the shelf prevent SACW from reaching the surface on the shelf (Figures 3b and 3c).

[15] In summer, relatively cold ($T < 18$°C, Figure 3d) and salty ($S > 35.5$, Figure 3e) SACW being upwelled from depths around 150 m reach the surface [*Möller et al.*, 2008]. In the upper layer, the density decreases offshore (Figure 3f). A virtually identical situation was observed off Torres (stations 71–76 in Figure 1, not shown), with the upwelling front placed some 20 km from the coast. The Torres and CSM sections were occupied between 14 and 15 February 2004. For the northernmost section (Itajaí/Bombinhas, stations 85–90 in Figure 1), the temperature and salinity distribution present strong vertical gradients with SACW placed at 20 m depth. The coastal stations of this section were occupied on 17 February, and SW winds were blowing since 15 February, forcing downwelling.

[16] From the above analysis, two distinct distributions are observed: in winter, the Plata plume is present, while in summer, the plume is retracted to the south, and upwelling events are more likely to occur. Though several studies have focused their attention on the properties and behavior of the Plata plume [e.g., *Piola et al.*, 2000; *Piola and Romero*, 2004; *Piola et al.*, 2008b; *Möller et al.*, 2008], no studies have previously described the CSM upwelling or discussed its dynamical balance. In the next section, we explore such events in terms of their synoptic variability.

3.2. Synoptic Variability of Upwelling Events

[17] Figure 4 presents the wind, temperature, and salinity time series recorded during a 7 day period in October 1973, when R/V *Alte*. *Saldanha* was moored collecting three hourly hydrographic profiles in the vicinity of CSM (indicated in Figure 1). To describe the response of the vertical structure to changes in the wind field, the wind record starts 80 h before the first vertical profile was collected (Figure 4a). Figure 4 indicates that upwelling events, considered here as the upward movement of the SACW until the time it starts downwelling, occur in pulses similar to those observed in Cape Frio [*Miranda*, 1982]. The onset of upwelling is controlled by NE winds, while downwelling starts immediately after the wind rotates to the SW due to the passage of a cold front (e.g., 24 October, Figure 4). The impact of changes in the alongshore winds on stratification is evident in the vertical displacement of the 18°C (Figure 4b) and 35 (Figure 4c)

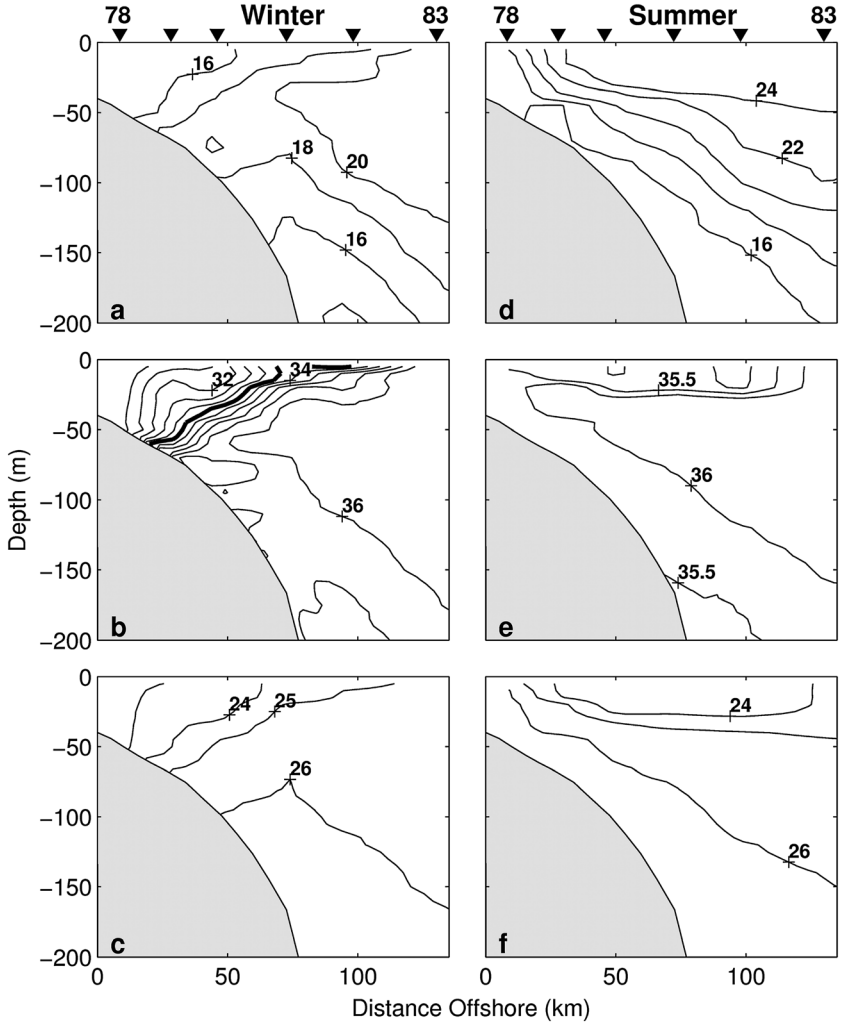

Figure 3. CSM transects (stations 78–83 in Figure 1) of temperature, salinity, and density for (a–c) winter and (d–f) summer. The bold contour in Figure 3b indicates the 33.5 isohaline. Inverted triangles on the top axis indicate the position of the hydrographic stations. Contour interval is 2°C for Figures 3a and 3d, 0.5 for Figures 3b and 3e, and 1 kg m^{-3} for Figures 3c and 3f.

isopleths. The first event probably lasted more than 40 h, with SACW reaching waters shallower than 10 m during this period, because winds were from NE since around 20 October. The second event took place after 28 October and lasted for about 40 h. The 18°C isotherm starts to rise some 20–30 h after the wind rotated to the NE, but did not reach the surface. This is due to the fast response of the water column to the abrupt wind change to the SE in October 30, which leads to downwelling of SACW. Vertical velocities were estimated from the vertical displacement of 16.5°C, 17°C, 17.5°C, and 18°C isotherms. On average, upward velocities were around 3×10^{-4} to 5×10^{-4} m s^{-1} (25.9–43.2 m day^{-1}), while downward velocities fluctuated from 8×10^{-4} to 11×10^{-4} m s^{-1} (69.1–95 m day^{-1}).

[18] It is interesting to note that after 28 October, when upwelling relaxes, warm ($T \sim 20$°C) and low-salinity waters ($32.5 < S < 34$) occupy the upper layer. With a single-point measurement, it is difficult to establish the origin of this water. The time series observations were obtained in late October, so it seems unlikely that the low salinities are derived from the Plata plume [see *Piola et al.*, 2008b, Figure 4]. The only other possible source of low-salinity waters is the Itajaí River, whose mouth is located near 26°55′S (see Figure 1 for reference). The low-salinity tongue ($S < 35.25$) extending southward from the mouth of the Itajaí river along the middle-shelf region observed in the summer distribution of surface salinity (Figure 2d) seems to confirm this hypothesis.

[19] The stratification time series reveals that the wind plays a key role in setting up the upwelling events in CSM. In the following section, we assess the relative importance of Ekman transport, Ekman pumping, and the interaction of the wind forcing with the changes in coastline orientation and shelf width.

3.3. Wind Effects on the Occurrence of Upwelling Events

[20] The cross-shore Ekman transport and Ekman pumping along the coast calculated for spring and summer are shown in Figure 5. Upwelling favorable (offshore) Ekman transport per meter along the coast is more intense (~0.5 m^3 s^{-1}) south of the cape, in both spring (Figure 5a) and summer (Figure 5b). The coastline orientation changes from N-S north of CSM to NE-SW south of the cape, thus becoming parallel to the NE

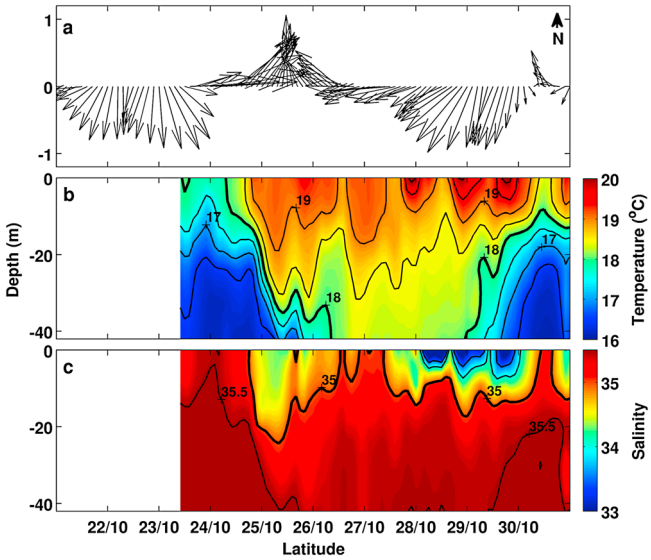

Figure 4. Time series of (a) wind vectors (stick plot) from reanalysis (RNA-II), (b) temperature, and (c) salinity measured during the repeated cast collected on R/V *Alte. Saldanha* (48.46°W and 28.37°S). The 18°C and 35 isopleths are highlighted to identify SACW. Contour intervals are 0.5 in both panels.

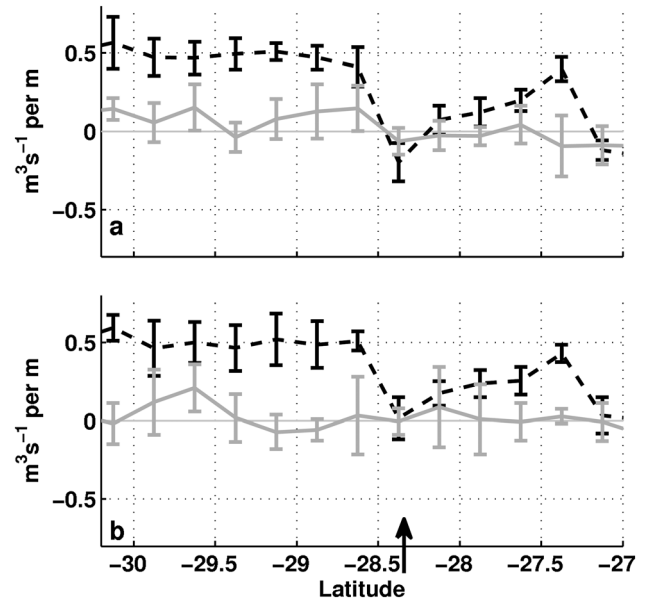

Figure 5. Seasonal Ekman transport (black line) and pumping (gray line) estimated for (top) spring and (bottom) summer along the coast near CSM. The arrow on the bottom axis indicates the location of CSM. Positive values indicate offshore (i.e., upwelling favorable) transport. The seasonal climatology is derived from QuikSCAT data spanning the period from 2003 to 2007.

wind field. This change in the coastline orientation seems to play a significant role in enhancing the offshore Ekman transport that leads to stronger upwelling south of CSM. Ekman transport and pumping were also estimated based on Blended Seawinds wind climatology (http://www.ncdc.noaa.gov/oa/rsad/air-sea/seawinds.html), in which wind speeds are derived from merging various satellite scatterometers and the directions come from the NCEP_Reanalysis 2 data provided by the NOAA/OAR/ESRL PSD, Boulder, CO (http://www.esrl.noaa.gov/psd/data/gridded/data.ncep.reanalysis2.html). The results present very similar patterns to those based on QuikSCAT data. Ekman pumping based on either of these wind products does not appear to play a significant role in the generation of upwelling events in CSM. This is in contrast with what is observed in Cape Frio, where it has been suggested that Ekman pumping accounts for about 50% of the total upwelling [*Castelão and Barth*, 2006]. Upwelling estimated in the California Current system also suggests that Ekman pumping is as important as Ekman transport from alongshore winds [*Picket and Paduan*, 2003]. The differences between CF and CSM areas are possibly associated with a change in the coastline orientation, which are smaller in the latter, leading to a weaker wind stress curl and, thus, a weaker contribution from the Ekman pumping to coastal upwelling.

[21] The above analysis suggests that offshore Ekman transport might control the upwelling core located south of CSM (Figure 2b). Other studies have suggested that variations in the bathymetry [*Song and Chao*, 2004; *Oke and Middleton*, 2000] and changes in coastline orientation [*Rodrigues and Lorenzetti* 2001] could also account for upwelling location as well as its intensity. In the following section, we use numerical simulations to further analyze these issues.

3.4. The Influence of Changes in Topography and Coastline Orientation

3.4.1. Numerical Model Results

[22] In this section, we examine the results generated by the model with full forcing (E1) focusing first on the surface circulation and then the subsurface circulation using selected cross sections. To supplement the discussion, the monthly mean wind stress vectors employed to force the model are shown in Figure 6. The surface salinity and temperature distributions derived from the model for winter (July monthly mean, Figures 7a and 7b) and summer (January monthly mean, Figures 7c and 7d) agree with results reported by previous studies [*Piola et al.*, 2000, 2005, 2008a, 2008b; *Möller et al.*, 2008]. In winter, a low-salinity and temperature tongue extends northward due to the prevailing southwesterly winds and associated northeastward flow (Figures 6a and 7a). In summer, the wind veers toward the northeast, the flow over the shelf reverses, and the low-salinity plume retracts southward to approximately 32°S (Figures 6b and 7d). The plume retraction in the summer simulation is similar to climatological and synoptic observations [e.g., *Piola et al.*, 2000; *Möller et al.*, 2008]. Two cores of relatively low surface temperature ($T < 19$°C) develop near the coast, one located south of CSM and one off Torres (Figure 7c), accompanied by a relatively sharp temperature decrease (from 25°C to 21°C) in a large part of the inner shelf. Given that the surface flow over the shelf is primarily southward and should advect warm TW from the north, the observed temperature drop can only arise from the upwelling of cold subsurface SACW. Since the pattern is not observed north of CSM, we hypothesize that it is associated with the change in coastline orientation and shelf width relative to the northeasterly prevailing winds. The satellite SST climatology in January shows that the South

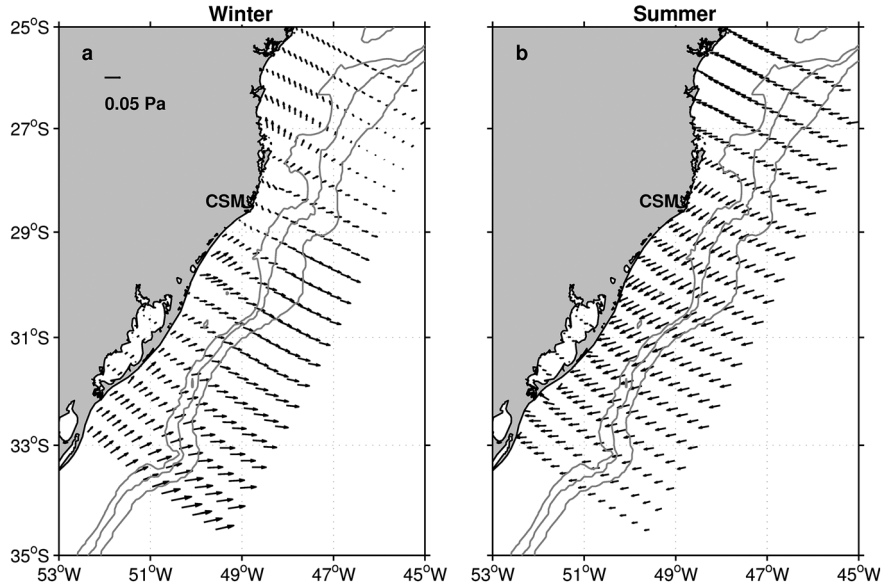

Figure 6. SCOW climatological wind stress for (a) winter (July monthly mean) and (b) summer (January monthly mean). Arrows indicate the wind stress with scale shown in Figure 6a, and the gray lines indicate 100, 200, and 1000 m isobaths.

Brazil Bight presents SST > 26°C, while south of CSM, SST < 25°C (Figure 8). This temperature change appears to be somewhat smaller than that produced by the model, but this may be a consequence of forcing the model with the climatological winds.

[23] To complement the above description and to explore the northward asymmetry in the summer SST distribution near CSM, we present three cross-shore transects: north (Figures 9a, 9d, and 9g), near CSM (Figures 9b, 9e, and 9h), and south of the cape (Figures 9c, 9f, and 9i). As the main goal of this paper is to analyze upwelling events, only the summer sections are presented. Winter cross-shore distributions (not shown) are very similar to that observed during Plata winter cruise (Figure 3) when southwesterly winds prevent upwelling. In summer, the influence of SACW on the inner shelf increases toward the south. The larger penetration of the cold and less saline SACW in the southern transect is marked by the surface outcropping of the 18°C isotherm (Figure 9c) and the inshore position of the 35 isohaline (Figure 9f). As we shall show, these water masses are first uplifted to the middle shelf by the BC and then brought to the surface by wind forcing. The cross-shelf circulation indicates large changes from the northern toward the southern sections. In the north, the onshore flow and upwelling is restricted to the bottom boundary layer (BBL), and there is a generalized offshore flow in the rest of the water column (Figure 9g). Off CSM, there is strong shelf-break upwelling, and the onshore flow in the BBL is relatively stronger (Figure 9h), being compensated by a weaker offshore flow in the water column above. The surface flow extends the relatively low-salinity shelf waters offshore, while below a subsurface layer of salty TW is observed in the middle shelf (Figure 9e). In the southern transect, cross-shore velocities are divergent in most of the water column at ~70 km offshore (Figure 9i), indicating the presence of an upwelling center in the middle shelf. With the exception of a shallow surface layer, inshore from this location, there is a strong onshore flow in the interior that sustains intense coastal upwelling. As we shall see below, the large part of SACW is upwelled at the CSM shelf break where the shelf narrows, is funneled southward by the alongshore flow, and is further entrained inshore by the flow divergence observed south of the cape.

3.4.2. The Synergy Between BC and Wind Forcing

[24] The summer occurrence of cold bands of SACW in the coastal surface layer south of CSM is clearly promoted by the synergy between shelf-break upwelling and wind forcing and enhanced by their interaction with the changes in coastline orientation and shelf width. To evaluate the relative contribution of the BC and wind forcing and unravel the physical mechanisms involved, we constructed an additional experiment (E2) using the same model setup as E1 but without tidal and wind forcing. Therefore, in E2, the shelf circulation is largely attributed to the influence of the deep circulation (BC current) imposed at the northern boundary of the model.

[25] To characterize the differences between E1 and E2, Figure 10 displays horizontal sections of the initial state and the two experiments. In the initial state, SSTs are nearly uniform throughout the domain, while the bottom temperatures decrease toward the shelf break (Figures 10a and 10d). The 17°C isotherm, which marks the transition between the cold SACW waters carried by the BC and the warmer shelf waters, roughly follows the 200 m isobath (Figure 10d). The middle panels of Figure 10 show the results of E2. The surface circulation is dominated by the strong southwestward flow of the BC over the continental slope and a weak northward flow inshore of the 100 m isobath (Figure 10b). The SST field is nearly uniform over the shelf with a slight increase of temperatures toward the shelf break (Figure 10b). The differences with the initial conditions are associated with the summer heating of the surface layer and the southward advection of warmer TW by the BC. The bottom temperatures show an overall drop of ~7°C from their initial state (Figure 10e), with

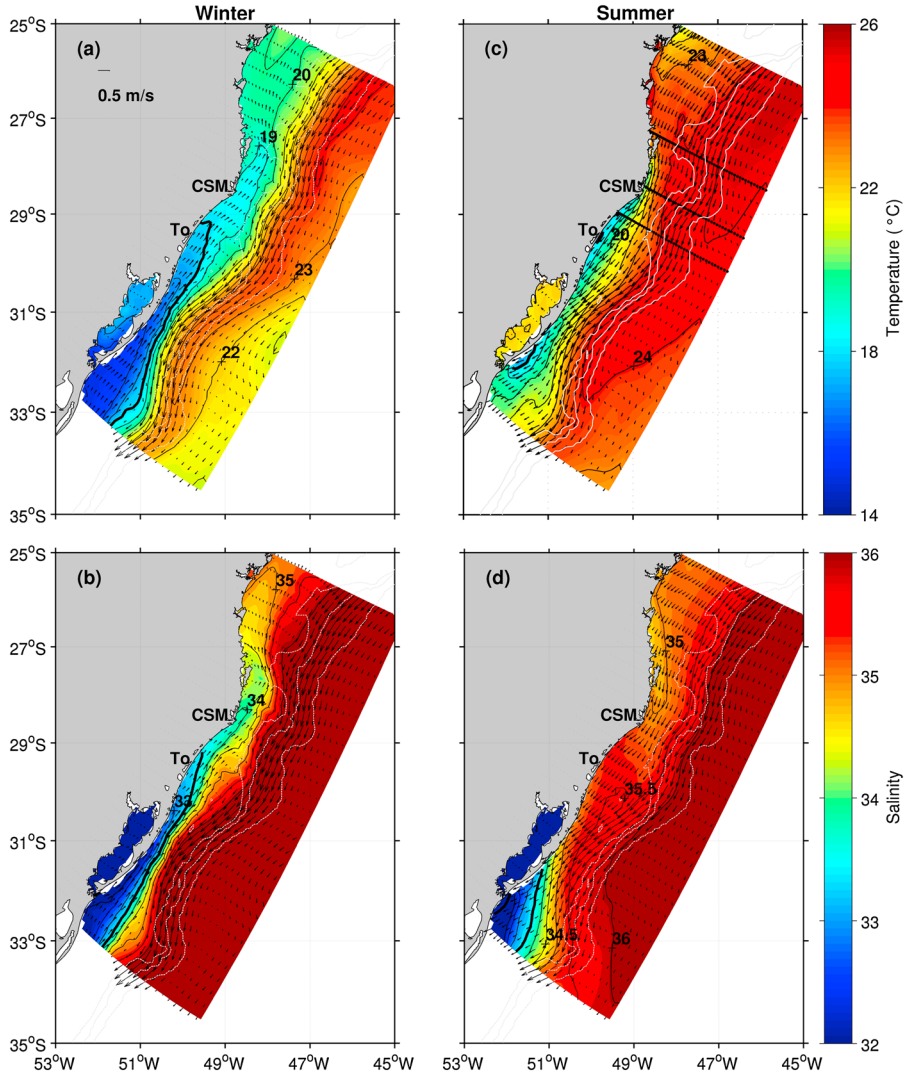

Figure 7. (left) Winter (July monthly mean) and (right) summer (January monthly mean) surface distributions of (a, c) temperature and (b, d) salinity from experiment E1. Arrows indicate the surface velocity (m s^{-1}) with scale shown in Figure 7a, and the white dashed lines indicate the 100, 200, and 1000 m isobaths. The bold contours indicate the 18°C isotherm in Figures 7a and 7c and the 33.5 isohaline in Figures 7b and 7d. Black lines in Figure 7d indicate the cross sections illustrated in Figure 9.

a marked along-shelf gradient that is characterized by the lowest values at CSM, where the shelf width attains a minimum. The contribution of the BC intrusions to the shelf water mass structure is exemplified by the inshore excursion of the 17°C isotherm, from its initial position near the 200 m isobath to a depth of 40 m throughout the shelf (Figure 10e).

[26] The influence of the wind stress forcing on the water mass structure and circulation of the CSM region is evident from the comparison of E1 and E2. Upwelling favorable winds in E1 further entrain the relatively cold waters of the BC onto the inner shelf near CSM and force the outcrop of deep, cold waters in the south (Figure 10c). The bottom circulation shows that the cold waters entrained near CSM are transported southward and then inshore of the 100 m isobath (Figure 10f).

3.4.3. Dynamical Analysis

[27] To further quantify the influence of onshore intrusions of the BC and the wind-driven component of the coastal upwelling, we computed the alongshore momentum balance

$$\underbrace{\frac{1}{D}\frac{\partial (DV)}{\partial t}}_{\text{CORY}} \underbrace{- fU}_{\text{PGY}} + \frac{\partial P}{\partial y} + \underbrace{\frac{1}{D}\frac{\partial}{\partial \sigma}\left(\frac{K_M}{D}\frac{\partial V}{\partial \sigma}\right)}_{\text{ZDY}} + \underbrace{A_y}_{\text{ADVY}} = 0 \quad (3)$$

where U and V are the horizontal velocity components, f is the Coriolis vector, P is the pressure, D is the water depth, σ is the sigma coordinate, K_M is the coefficient of vertical viscosity, and A_y collects all the terms related to advection and horizontal diffusion. It is also convenient to split the total pressure gradient into its barotropic and baroclinic parts, i.e.,

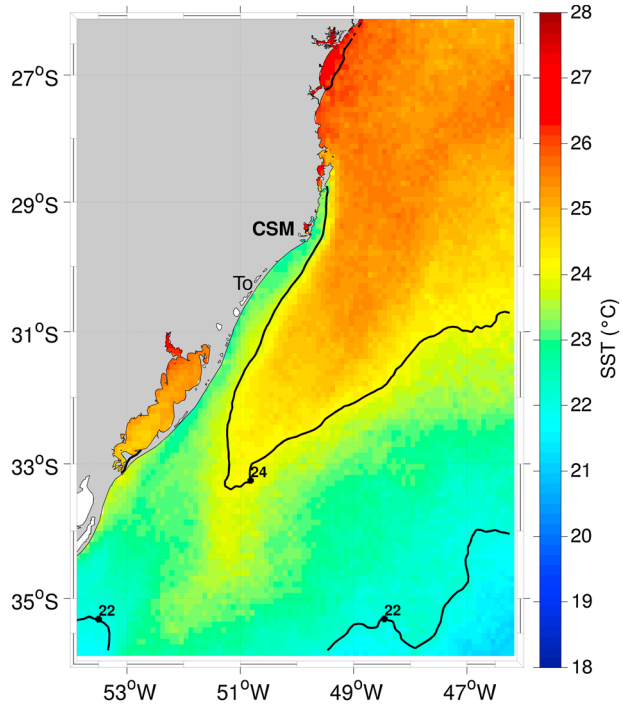

Figure 8. Summer (January monthly mean) SST climatology derived from MODIS-Aqua 9 km resolution data spanning the period from 2003 to 2007.

$$\frac{\partial P}{\partial y} = \overset{\text{EGY}}{g\frac{\partial \eta}{\partial y}} + \overset{\text{BGY}}{g\frac{\partial \Phi}{\partial y}} = g\frac{\partial \eta}{\partial y} + g\frac{D}{\rho_o}\int_{\sigma}^{0}\left[\frac{\partial \rho}{\partial y} - \frac{\sigma}{D}\frac{\partial D}{\partial y}\frac{\partial \rho}{\partial \sigma}\right]d\sigma \qquad (4)$$

where g is gravity, η is the surface elevation, and ρ is the density. The horizontal momentum balance of E2 in the BBL (averaged over the last two sigma levels) is dominated by the along-shelf pressure gradient (EGY + BGY), the Coriolis term (CORY), and vertical diffusion (ZDY) (Figure 11, left panels). Their spatial variations identify the dynamical mechanisms that regulate the shelf-break upwelling in the different portions of the study region. Slightly north of CSM, the balance is controlled by the barotropic component of the along-shelf pressure gradient (EGY), which, through geostrophy, generates intense upward and inshore velocities near the 200 m isobaths and, hence, the strongest shelf-break upwelling center (Figures 11a and 11b). As noted in *Palma and Matano* [2009], this particular balance reflects the along-shelf variations of the coastline and bottom topography since, without them, a classical Ekman balance between vertical diffusion and the Coriolis term would dominate the BBL. The increase in vertical diffusion off CSM reflects the bottom flow acceleration near the shelf break (Figures 10e and 11d). Coastline orientation changes in the northern and southern portions of the CSM region lead to a change of sign of the alongshore pressure gradient and, hence, to offshore velocities

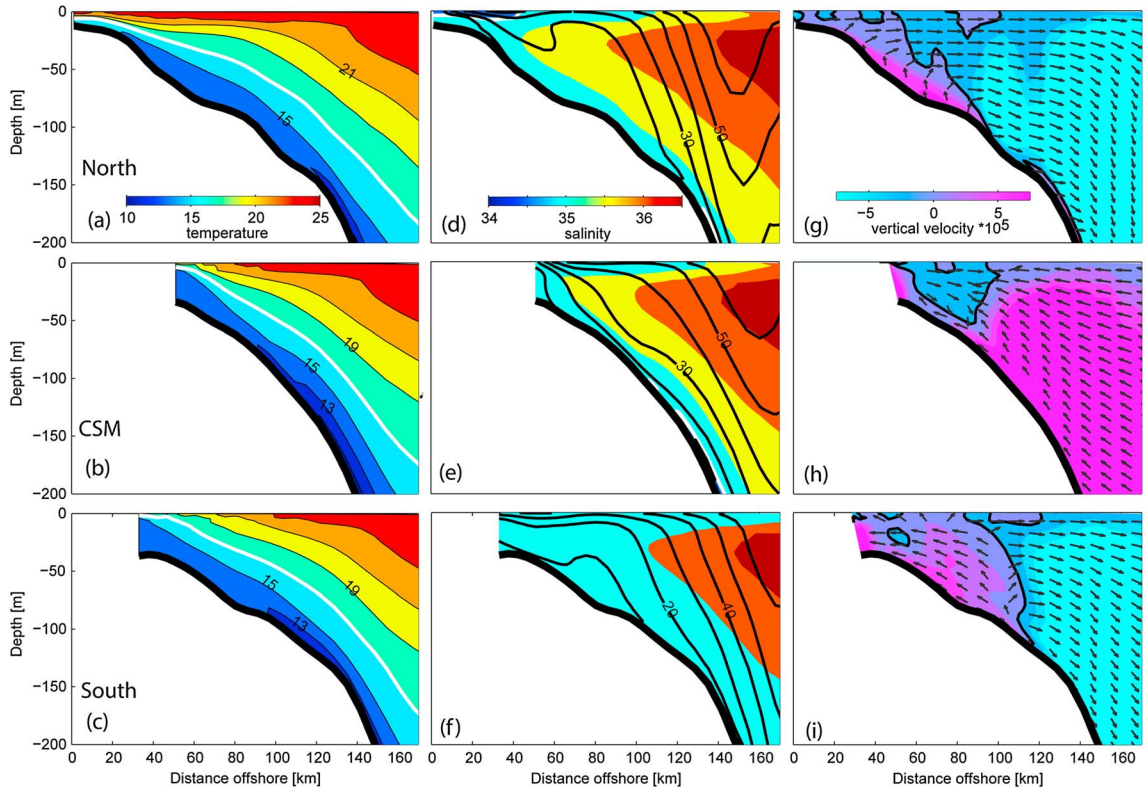

Figure 9. Summer (January monthly mean) cross-shore sections of (a–c) temperature, (d–f) salinity (colors) and alongshore velocity (black contours), and (g–i) cross-shore velocity vectors (vectors indicate only flow direction) and vertical velocity (colors) from experiment E1. The thick white line in the left panels indicates the 17°C isotherm. Full contours in the middle panels indicate the southward flow (CI: 10 cm/s) Each panel displays the sections (top) north, (middle) off CSM, and (bottom) south of the cape. See Figure 7 for section locations.

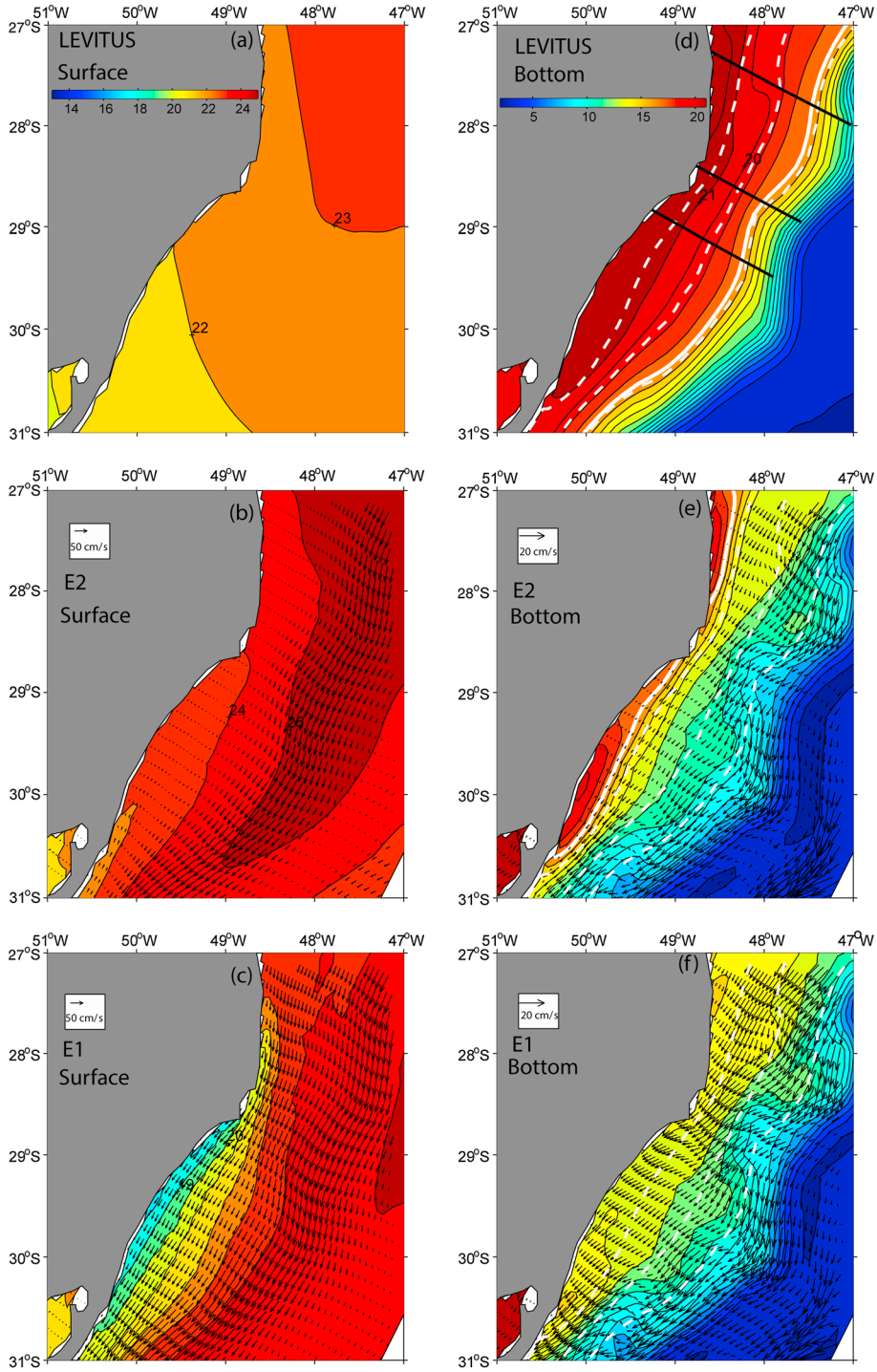

Figure 10. (left) Summer (January monthly mean) sea surface temperature and surface velocity vectors: (a) initial condition, (b) E2 results, and (c) E1 results. (right) Bottom temperature and velocity vectors: (d) initial condition, (e) E2 results, and (f) E1 results. White dashed lines indicate the 50, 100, and 200 m isobaths. The bold white line indicates the position of the 17°C isotherm. Black lines in Figure 10d indicate the cross sections illustrated in Figure 9.

(i.e. downwelling) in the BBL of the shelf break (Figures 11a and 11b).

[28] The contribution of wind stress forcing to the momentum balance is illustrated in the right panels of Figure 11 and complemented with selected cross-shelf sections in Figure 12. The largest changes brought by the summer wind stress forcing in the BBL are felt both locally and regionally inshore of the 100 m isobaths (Figure 11, right panels). There is not only a local increase in the bottom flow driven by the southerly winds (Figure 11e) but also a significant regional change in the barotropic pressure gradient (EGY) both north and south of CSM (Figure 11f). The change in sign in the EGY field

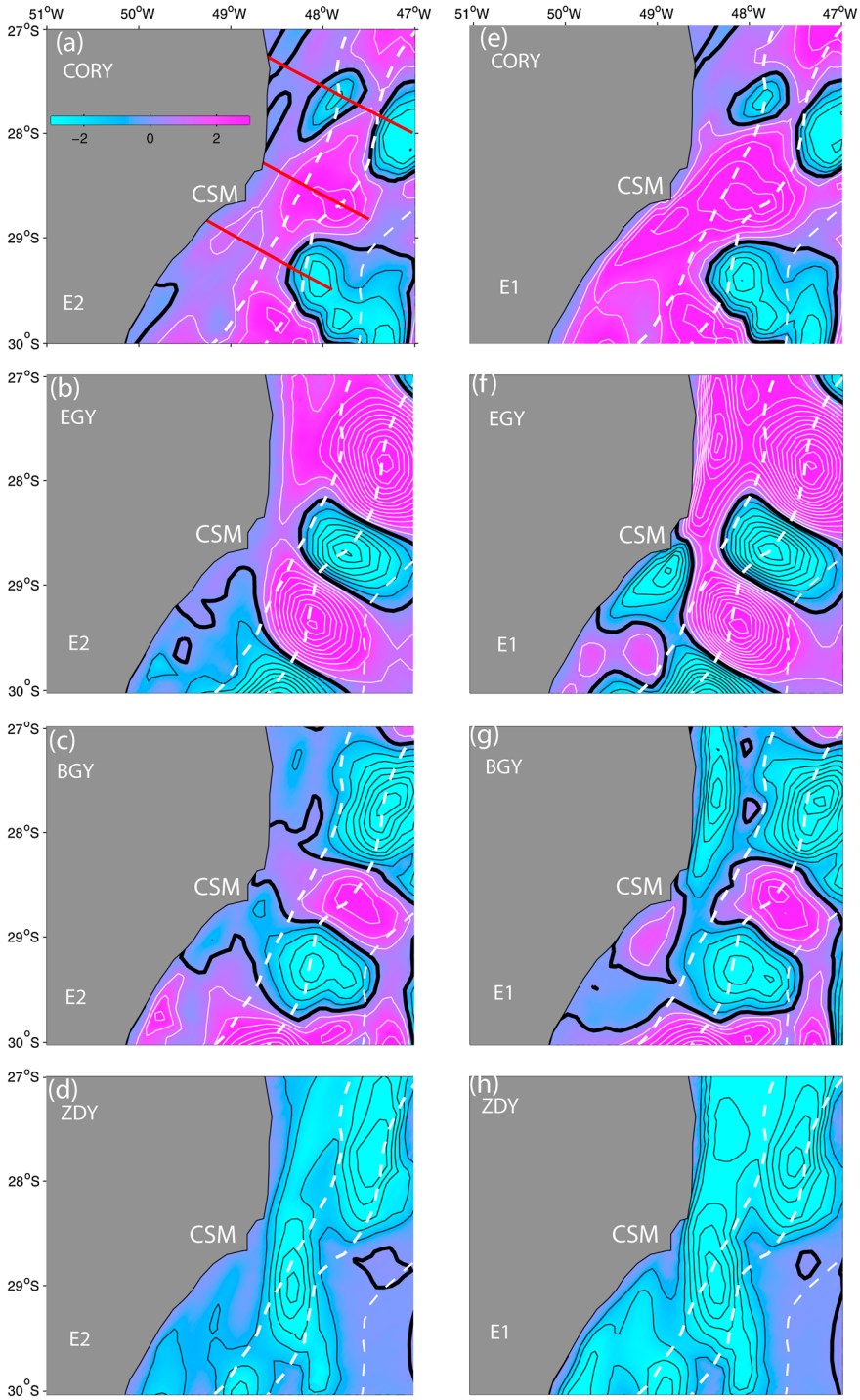

Figure 11. Summer (January monthly mean) momentum balance in the BBL for (left) E2 (BC forcing and (right) E1 (full forcing). CORY (Coriolis term, positive values indicate inshore flow), EGY (barotropic pressure gradient), BGY (baroclinic pressure gradient), and ZDY (vertical diffusion). White dashed lines indicate the 100, 200, and 1000 m isobaths. Red lines in Figure 11a indicate the cross sections illustrated in Figure 12.

reflects the convergence and divergence of the flow field north and south of CSM, respectively (Figure 10c). The slope water uplifted at the CSM section by the favorable pressure gradient is further entrained toward the coast by the intensification of the bottom flow (Figures 12e and 12h). Part of this water recirculates nearshore and is funneled toward the southwest and upwelled farther south in the near-coastal region (Figures 10c and 10f). With the exception of a thin surface layer, the upwelling process in the southern sector is sustained by onshore flow driven in the entire water column by the

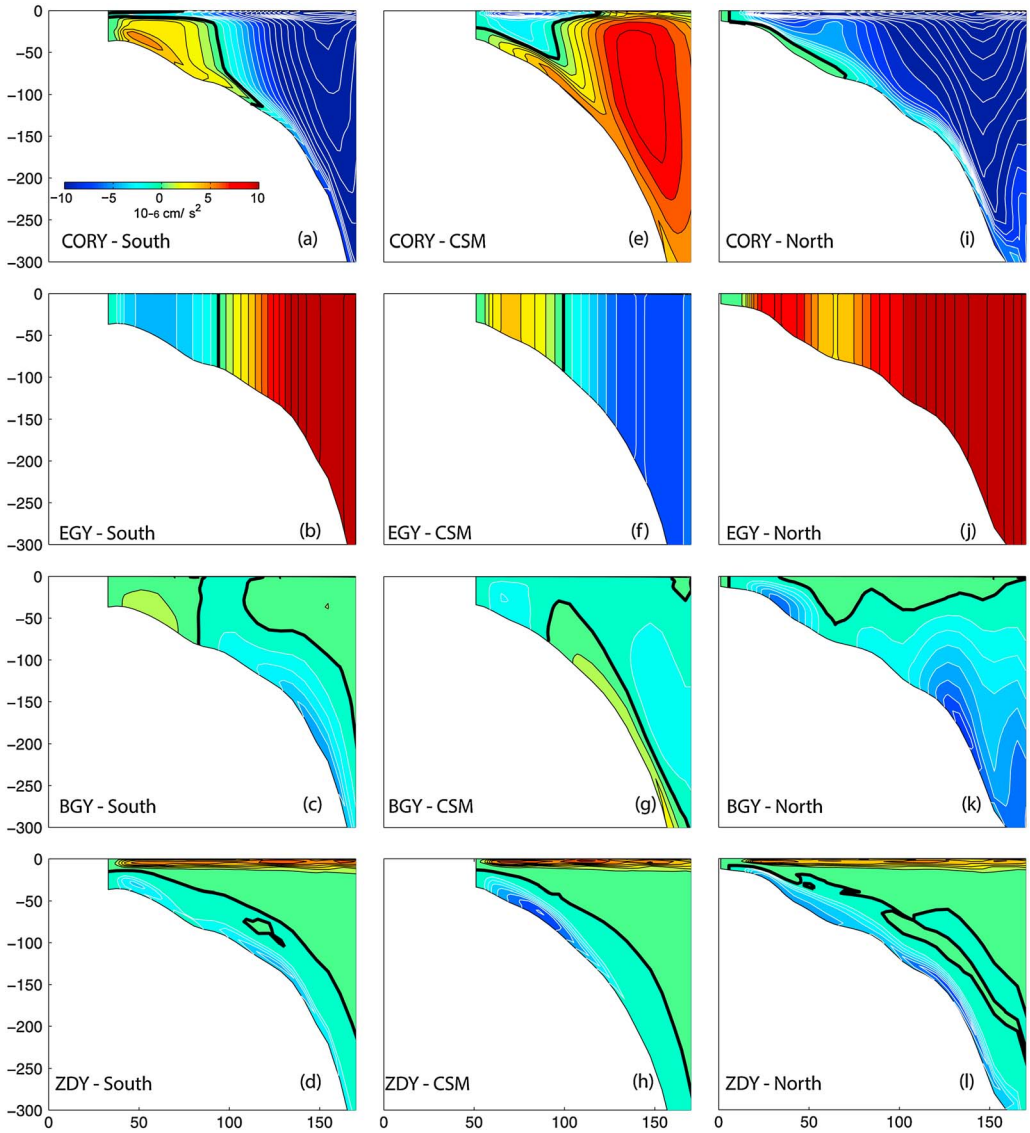

Figure 12. Summer (January monthly mean) along-shelf momentum balance for experiment E1 (full forcing) at three selected cross sections located south, at, and north of CSM (see Figure 11). CORY (Coriolis term, positive values indicate inshore flow), EGY (Barotropic pressure gradient), BGY (baroclinic pressure gradient), and ZDY (vertical diffusion).

favorable barotropic pressure gradient (Figure 12b). The zero line of the CORY plot in Figure 12a marks the location of convergence of the subsurface and bottom velocities and, hence, a secondary inner shelf upwelling center (Figure 9i). In the northern region, although the addition of wind forcing leads to an increase in vertical mixing and inshore bottom flow in the BBL (Figure 12l), the pressure gradient changes sign, and there is predominant offshore flow and, hence, downwelling in almost the entire water column (Figures , 9g, 12i, and 12j). In summary, there is shelf-break upwelling near the CSM location but shelf-break downwelling north and south of the cape. However, the increase in the southward flow generated by the northeasterly winds in conjunction with the middle-shelf flow divergence promoted by the shelf expansion drives an inshore flow that enhances the observed coastal upwelling south of the cape.

4. Discussion

[29] The results presented here highlighted the large seasonal variability of water mass distribution and circulation associated with changes in the wind field on the southern Brazil continental shelf between 31°S and 26°S. Changes in wind direction modulate the meridional displacements of PPW [*Piola et al.*, 2005], creating two distinct oceanographic conditions: with and without the presence of PPW. In winter, the inner shelf is characterized by northward flow which advects low-salinity waters ($S < 33$) from the Plata, while in summer, alongshore velocities reverse, and north of about 32°S, the salinity increases substantially ($S > 35$), and its distribution becomes highly homogeneous. Similar patterns of surface salinity and circulation have been reported in previous studies based on the analysis of hydrographic data

[e.g., *Piola et al*., 2000], satellite imagery [*Piola et al*., 2008b], and numerical simulations [*Palma et al*., 2008].

[30] This strong seasonal signal is not observed in the outer shelf. Both our hydrographic data and model simulations indicate the yearlong presence of shelf-break upwelling induced by interactions of the BC with the bottom topography in the outer shelf. The shelf-break upwelling mechanism forces SACW onto the shelf, while northeasterly winds enhance coastal upwelling during spring and summer at distinct locations. For example, previous studies suggest that NE winds reinforce the effect of shelf-break upwelling, bringing SACW closer to the surface in the northern sector of the South Brazil Bight [*Campos et al*., 1995, 2000; *Palma et al*., 2008; *Palma and Matano*, 2009]. The wind action associated with shelf-break upwelling has been also reported elsewhere. *Gibbs et al*. [1998] concluded that the most favorable conditions for coastal upwelling in the Sydney region occur when an intrusion of East Australian Current precedes a prolonged northerly wind period.

[31] Summer surface temperature distributions from hydrographic data and numerical simulations (Figures 2c and 7c) indicate that coastal upwelling off CSM is centered south of the cape. A preliminary examination of the wind data base indicated that one of the factors explaining this asymmetry could be related to the increase of the inner shelf wind-driven Ekman transport. However, analysis of the numerical experiments showed that this particular location of the upwelling band is related to the synergy between shelf-break upwelling and the regional shelf circulation induced by the northeasterly winds. On one hand, the narrowing of the shelf off CSM promotes a larger intrusion of SACW in the middle shelf at this location. On the other hand, the increase in the southward flow generated by the northeasterly winds in conjunction with the middle-shelf flow divergence promoted by the widening shelf drives an inshore flow that enhances the coastal upwelling south of the cape.

[32] Studies have shown that bathymetric variations [*Oke and Middleton*, 2000] and changes in coastline orientation [*Rodrigues and Lorenzzetti*, 2001] may also play a significant role in determining the upwelling location and intensity in other shelf regions. *Rodrigues and Lorenzzetti* [2001] suggested that the coastline orientation plays a key role in the magnitude of upwelling events in Cape Frio, while topographic variations control upwelling near Cape São Tomé. More recently, using a numerical simulation quite similar to the one used in this study, *Matano et al*. [2010] have suggested that changes in the continental shelf width can reverse the direction of the along-shelf pressure gradient, thus affecting shelf-break upwelling/downwelling. Using a simplified numerical simulation of the California upwelling system, *Gan and Allen* [2002] found that, downstream of capes, alongshore currents tend to separate from the coast and that the coldest surface water is found at those locations. This is in agreement with the more conspicuous observation of upwelling cores south of CSM (e.g., downstream in summer). *Li and Weisberg* [1999] also observed an intensification of the upwelling in the lee of capes along western Florida continental shelf. Hence, the location of an upwelling core south of CSM in summer appears to agree with most of the above-mentioned studies.

[33] Another important feature of the upwelling events near CSM is its occurrence in pulses associated with changes in the wind field. The response time to northeasterly winds is about 20–30 h, while the changes in stratification seem to respond faster to winds from the SW. Upwelling velocities inferred from vertical isopleths displacements ($w \sim 4 \times 10^{-4}$ m s^{-1} or ~34.5 m day^{-1}) are similar to those estimated by *Ikeda* [1976] ($w = 6.9 \times 10^{-4}$ m s^{-1} or ~59.5 m day^{-1}) during an upwelling event in Cape Frio associated with 8 m s^{-1} winds. The numerical simulations with realistic coastline and topography of *Rodrigues and Lorenzzetti* [2001]forced by 6 m s^{-1} winds led to a mean upwelling velocity of 4.7×10^{-4} m s^{-1} (~40.5 m day^{-1}). Estimates of vertical velocity based on the displacement of the 18°C isotherm off Cape Frio indicated upwelling velocities varying from 0.3×10^{-4} to 0.8×10^{-4} m s^{-1} (~2.5–7 m day^{-1}), while downwelling velocities were 1 order of magnitude larger [11×10^{-4} m s^{-1} or ~95 m day^{-1}, *Valentin et al*., 1987], but similar to those found in this study. In the Peruvian upwelling area off San Juan, the largest upwelling velocities estimated by *Brink et al*. [1981] were 4×10^{-4} m s^{-1} (~34.5 m day^{-1}).

5. Summary and Conclusions

[34] The coastal ocean near Cape Santa Marta presents strong seasonal variability, being under the influence of (a) low-salinity waters derived from the Rio de la Plata during austral fall and winter and (b) upwelling events interspersed with the presence of STSW during spring and summer. Coastline and bathymetry variations and seasonal and synoptic changes in wind direction lead to these changes in water mass composition and in the horizontal and vertical structures of water properties. The narrowing of the continental shelf off CSM and the further widening of the shelf farther south allows the BC to feed the bottom shelf with cold SACW upwelled at the shelf break throughout the year. Coastal upwelling events, however, occur only under the influence of favorable winds. These events occur in pulses associated with changes in wind direction and are more evident in the area south of the cape. The proposed physical mechanism is related to the increase in the southward flow generated by the northeasterly winds in conjunction with the middle-shelf flow divergence promoted by the shelf widening downwind. This flow divergence drives an inshore flow that enhances the coastal upwelling south of the cape. Northeasterly, upwelling favorable, winds are more frequently observed in late austral spring and summer. The higher intensity of Ekman transport driven by northeasterly winds south of CSM appears to be due to the change in the coastline orientation and the variations in the shelf width.

[35] **Acknowledgments.** The PLATA project was financed by the Inter-American Institute for Global Change Research (IAI) grant CRN061 and CRN2076 through the U.S. National Science Foundation grant GEO-0452325 and by Naval International Cooperative Opportunities in Science and Technology Program grant from the U.S. Office of Naval Research (grant N00014-02-1-0295). E.D.P. acknowledges the financial support from CONICET (PIP09-112-200801), Agencia Nacional de Promoción Científica y Tecnológica (PICT08–1874), and Universidad Nacional del Sur (24F044). We also acknowledge the crews of R.V. N.Oc. *Antares* and A.R.A. *Puerto Deseado* and the scientific parties for valuable assistance during each cruise, as well as Conselho Nacional de Desenvolvimento Científico e Tecnológico (CNPq) for grant 302231/2010-2 (O.M.J.). P.C.C. acknowledges SACC/IAI (CRN 2076, grant GEO-0452325)) and Coordenação de Aperfeiçoamento de Pessoal de Nível Superior (CAPES). We gratefully acknowledge two anonymous reviewers for their helpful comments on the manuscript.

References

Blumberg, A. F., and G. L. Mellor (1987), A description of a three-dimensional coastal ocean circulation model, in Three-Dimensional Coastal Ocean Models, Coastal and Estuarine Science Series 4, edited by N. Heaps, pp. 1–16, AGU, Washington, D. C.

Brink, K. H., B. H. Jones, J. C. Van Leer, C. N. K. Mooers, D. W Stuart, M. R. Stevenson, R. C. Dugdale, and G. W. Heburn (1981), Physical and biological structure and variability in an upwelling center off Peru near 15°S during March 1977, in Coastal Upwelling, Coastal and Estuarine Sciences 1, edited by F. A. Richards, pp. 473–495 AGU, Washington, D. C.

Campos, E. J. D., J. E. Gonçalves, and Y. Ikeda (1995), Water mass characteristics and geostrophic circulation in the South Brazil Bight Summer of 1991, *J. Geophys. Res.*, *100*(C9), 18.537–18.550.

Campos, E. J. D., D. Velhote, and I. C. A. Da Silveira (2000), Shelf break upwelling driven by Brazil Current cyclonic meanders, *Geophys. Res. Lett.*, *27*, 751–754, doi:10.1029/1999GL010502.

Campos, E. J. D., A. R. Piola, R. P. Matano, and J. L. Miller (2008), PLATA: A Synoptic characterization of the southwest Atlantic shelf under influence of the Plata River and Patos Lagoon outflows, *Cont. Shelf Res.*, *28*, 1551–1555, doi:10.1016/j.csr.2008.03.007.

Carbonel, C. A. A. H. (2003), Modelling of upwelling–downwelling cycles caused by variable wind in a very sensitive coastal system, *Cont. Shelf Res. 23*, 1559–1578, doi:10.1016/S0278-4343(03)00145-6.

Castelão, R. M., E. J. D. Campos, and J. L. Miller (2004), A modelling study of coastal upwelling driven by wind and meanders of the Brazil Current, *J. Coast. Res.*, *20* (3), doi:10.2112/1551-5036(2004)20[662:AMSOCU]2.0.CO;2.

Castelão, R. M., and J. A. Barth (2006), Upwelling around Cabo Frio, Brazil: The importance of wind stress curl, *Geophys. Res. Lett.*, *33* (L03602), doi:10.1029/2005GL025182.

Castello, J. P., and O. O. Möller (1977), On the oceanographic conditions off Rio Grande do Sul, *Atlântica 2*(2), 25–110.

Egbert, G. D., A. F. Bennet, and M. G. Foreman (1994), TOPEX/POSEIDON tides estimated using a global inverse model, *J. Geophys. Res. 99*, 24,821–24,852, doi:10.1029/94JC01894.

Gan, J., and J. S. Allen (2002), A modeling study of shelf circulation off northern California in the region of the Coastal Ocean Dynamics Experiment: Response to relaxation of upwelling winds, *J. Geophys. Res.*, *107* (C9), doi:10.1029/2000JC000768.

Gibbs, M. T., J. H. Middleton, and P. Marchesiello (1998), Baroclinic response of Sydney Shelf waters to local and deep ocean forcing, *J. Phys. Oceanogr.*, *28*, 178–190, doi:10.1175/1520-0485(1998)028 < 0178:BROSSW > 2.0.CO;2.

Guimaraens, M. A., and R. Coutinho (2000), Temporal and spatial variation of *Ulva* spp. and water properties in the Cabo Frio upwelling region of Brazil, *Aquat. Bot. 66*, 101–114.

Ikeda, Y. (1976), Variações em escala média da temperatura e da salinidade do mar na região entre a Baía de Guanabara e Cabo Frio (17/08 a 26/08/1971), *Bol. Inst. Oceanogr. 25*, 221–280.

Li, Z., and R. H. Weisberg (1999), West Florida shelf response to upwelling favorable wind forcing: kinematics, *J. Geophys. Res.*, *104*, 13507–13527, doi:10.1029/1999JC900073.

Matano, R. P., E. D. Palma, and A. R. Piola (2010), The influence of the Brazil and Malvinas Currents on the southwestern Atlantic shelf circulation, *Ocean Sci.*, *6*, 983–995, doi:10.5194/os-6-983-2010.

Matsuura, Y. (1986), Contribuição ao estudo da estrutura oceanográfica da região sudeste entre Cabo Frio (RJ) e Cabo de Santa Marta Grande (SC), *Ciên. Cult. 38*(8), 1439–1450.

Matsuura, Y., (1998), Brazilian sardine (*Sardinella brasiliensis*) spawning in the Southeast Brazilian Bight over the period 1976–1993, *Rev. Bras. Oceanogr.*, *46*(1), 33–43.

Miranda, L. B., (1982), Análise de massas de água da plataforma continental e da região oceânica adjacente: Cabo de São Tomé (RJ) e Ilha de São Sebastião (SP), PhD thesis, Instituto Oceanográfico, Universidade de São Paulo, São Paulo, Brazil.

Möller, O. O. Jr., A. R. Piola, A. C. Freitas, and E. J. D. Campos (2008), The effects of river discharge and seasonal winds on the shelf off southeastern South America, *Cont. Shelf Res. 28*(13), 1607–1624, doi:10.1016/j.csr.2008.03.012.

Moser, G. A. O., and S. M. F. Gianesella-Galvão (1997), Biological and oceanographic upwelling indicators at Cabo Frio (RJ), *Rev. Bras. Oceanogr.*, *45* (1–2), 11–23.

Odebrecht, C., and L. Djurfeldt (1996), The role of nearshore mixing on phytoplankton size structure off Cape Santa Marta Grande, southern Brazil (Spring 1989), *Arch. Fish. Mar. Res. 43*(3), 217–230.

Oke, P. R., and J. H. Middleton (2000), Topographically induced upwelling off Eastern Australia, *J. Phys. Oceanogr. 30*, 512–531, doi:10.1175/1520485(2000)030 < 0512:TIUOEA > 2.0. CO;2.

Palma, E. D., and R. P. Matano (1998), On the implementation of open boundary conditions to a general circulation model: The barotropic mode, *J. Geophys. Res. 103*, 1319–1341.

Palma, E. D., and R. P. Matano (2000), On the implementation of open boundary conditions to a general circulation model: The 3-D case, *J. Geophys. Res. 105*, 8605–8627.

Palma, E. D., R. P. Matano, and A. R. Piola (2008), A numerical study of the Southwestern Atlantic Shelf circulation: Stratified ocean response to local and offshore forcing, *J. Geophys. Res. 113* (C11010), doi:10.1029/2007JC004720.

Palma, E. D., and R. P. Matano (2009), Disentangling the upwelling mechanisms of the South Brazil Bight, *Cont. Shelf Res. 29*, 1525–1534, doi:10.1016/j.csr.2009.04.002.

Pickett, M. H., and J. D. Paduan (2003), Ekman transport and pumping in the California Current based on the U.S. Navy's high-resolution atmospheric model (COAMPS), *J. Geophys. Res.*, *108* (C10), 3327, doi:10.1029/2003JC001902.

Piola, A. R., E. J. D. Campos, O. O. Moller Jr., M. Charo, and C. M. Martinez (2000), Subtropical shelf front off eastern South America, *J. Geophys. Res. 105* (C3), 6566–6578. doi:10.1029/1999JC000300.

Piola, A. R., and S. I. Romero (2004), Space-time variability of the Plata River Plume, *Gayana 68* (3), 482–486.

Piola, A. R., R. P. Matano, E. D. Palma, O. O. Moller Jr., and E. J. D. Campos (2005), The influence of the Plata River discharge on the western South Atlantic shelf, *Geophys. Res. Lett. 32* (L01603), doi:10.1029/2004GL021638.

Piola, A. R., O. O. Möller Jr., R. A. Guerrero, and E. J. D. Campos (2008a), Variability of the subtropical shelf front off eastern South America: Winter 2003 and summer 2004, *Cont. Shelf Res. 28* (13), 1639–1648, doi:10.1016/j.csr.2008.03.013.

Piola, A. R., S. I. Romero, and U. Zajaczkovski (2008b), Space-time variability of the Plata plume inferred from ocean color, *Cont. Shelf Res. 28* (13), 1556–1567, doi:10.1016/j.csr.2007.02.013.

Resgalla, C. Jr., C. De La Rocha, and M. A. Montú (2001), The influence of Ekman transport on zooplankton biomass variability off southern Brazil, *J. Plankton Res. 23*(1), 1191–1216.

Risien, M. R., and D. B. Chelton (2008), A global climatology of surface wind and wind stress fields from 8 years of QuikSCAT scatterometer data, *J. Phys. Oceanogr. 38* (11), 2379–2413, doi:10.1175/2008JPO3881.1.

Rodrigues, R. R., and J. A. Lorenzzetti (2001), A numerical study of the effects of bottom topography and coastline geometry on the Southeast Brazilian coastal upwelling, *Cont. Shelf Res.*, *21*, 371–394.

Smith, R. L. (1968), Upwelling, *Oceanogr. Mar. Biol. Annu. Rev. 6*, 11–46.

Smith, R. D., and D. T. Sandwell (1997), Global sea floor topography from satellite altimetry and ship depth soundings, *Science 277*, 1956–1962.

Song, Y. T., and Y. Chao (2004), A theoretical study of topographic effects on coastal upwelling and cross-shore exchange, *Ocean Modell. 6*, 151–176, doi:10.1016/S1463-5003(02)00064-1.

Tokmakian, R., and P. Challenor (1999), On the joint estimation of model and satellite sea surface height anomaly errors, Ocean Modell. 1, Hooke Inst. Oxford Univ., Oxford, U. K., 39–52.

Valentin, J. L., D. L. Andre, and S. A. Jacob (1987), Hydrobiology in the Cabo Frio (Brazil) upwelling: Two-dimensional structure and variability during a wind cycle, *Cont. Shelf Res.7* (1), 77–88.

Vaz, A. C., O. O. Möller, and T. L. Almeida (2006), Análise quantitativa da descarga dos rios afluentes da Lagoa dos Patos, *Atlântica*, *28*(1), 13–23.